Solution of the logarithmic Schrödinger equation with a Coulomb potential

Journal of Physics Communications

PAPER

Solution of the logarithmic Schrödinger equation with a Coulomb potential

T C Scott[1,2] and J Shertzer[3]

[1] Near Pte. Ltd, 15 Beach Road, 189677, Singapore
[2] Institut für Physikalische Chemie, RWTH Aachen University, D-52056 Aachen, Germany
[3] Department of Physics, College of the Holy Cross, 1 College St, Worcester, MA 01610, United States of America

E-mail: tcscott@gmail.com

Keywords: logarithmic Schrödinger equation, Gaussons, finite element methods

OPEN ACCESS

RECEIVED
5 June 2018

REVISED
4 July 2018

ACCEPTED FOR PUBLICATION
12 July 2018

PUBLISHED
24 July 2018

Abstract

The nonlinear logarithmic Schrödinger equation (log SE) appears in many branches of fundamental physics, ranging from macroscopic superfluids to quantum gravity. We consider here a model problem, in which the log SE includes an attractive Coulomb interaction. We derive an analytical solution for the ground state energy and wave function as a function of the strength of the logarithmic interaction. We develop an iterative finite element method to solve the Coulombic log SE for the spherically symmetric states. The ground state results agree with the exact solution to better than one part in 10^{10}. The excited states ($n>1$) are converged to better than one part in 10^{8}. We also construct a remarkably simple variational wave function, consisting of a sum of Gaussons with n free parameters. One can obtain an approximation to the energy and wave function that is in good agreement with the finite element results. Although the Coulomb problem is interesting in its own right, the iterative finite element method and the variational Gausson basis approach can be applied to any central force Hamiltonian.

1. Introduction

The logarithmic Schrödinger equation (log SE) is one of the nonlinear modifications of Schrödinger's equation, with applications in quantum optics [1, 2], nuclear physics [3, 4], diffusion phenomena [5], stochastic quantum mechanics [6], effective quantum gravity [7] and Bose–Einstein condensation [8, 9]. A relativistic version in the form of a Klein–Gordon type equation displaying dilatation/conformal covariance was first proposed by G. Rosen [10].

Bialynicki-Birula and co-workers investigated the log SE in the context of nonlinear wave mechanics [11–13]. Recently there has been more widespread interest in this highly nonlinear form of the Schrödinger equation. It has been hypothesized that superfluid vacuum theory (SVT) might be responsible for the mass mechanism (in contradistinction to the Higgs boson or perhaps working in tandem with it). Others have proposed connections between quantum gravity and Bose–Einstein condensates in the form of quantum liquids [14]. A version of SVT favors a logarithmic Schrödinger equation over a Gross-Pitaevski equation [9, 15]. In particular, the logarithmic model can account for the *upside-down Mexican hat shape of the Higgs potential* and its solution is claimed to be even more stable and energetically favorable than the model with a quartic (Higgs-like) potential [9, 16, 17]. Although the Higgs boson reported at 125 Gev has been confirmed, the Higgs potential has not been firmly established.

The reported resemblance between the gravitational dilaton and the Higgs boson [18] becomes all the more compelling because the log SE is a common feature. Thus, in the present work, we consider precise methods, both analytical and computational, for accurately solving the log SE. This not only serves as a sequel to our previous work in dilatonic quantum gravity [19] but provides the tools by which to make a number of alternate and future investigations with the log SE.

Herein, we consider a computational model consisting of a Coulomb potential with an additional logarithmic term for the following reasons:

(i) The electromagnetic interaction appears in proposed models for the Higgs potential [17].

(ii) The Newtonian and post-Newtonian gravitational potentials in the general relativistic model have the form $1/r^n$ [20, 21]; $n = 1$ corresponds to the case considered here.

(iii) The two-body dilatonic quantum gravity model [22], consisting of only one spatial dimension, leads to Coulombic terms for the more general dilatonic problem of [19] in three spatial dimensions.

The outline of this work is as follows. First, we present the log SE governing our model and the unusual nonorthogonality condition that results from the logarithmic term. The log SE with a Coulomb interaction has a simple analytic solution only for the ground state. This exact solution provides us with a benchmark by which to test our numerical methods.

Second, we present the computational details of the iterative FEM approach [23–25]. The finite element method has been successfully used to solve the Schrödinger equation for a variety of atomic and molecular systems, in 1D, 2D and even 3D. Based on a variational principle, it provides rigorous upper bounds to the energy. In particular, the FEM method succeeded in isolating the effect of a singularity structure at the Fermi level (10^{-15}m range) within a continuous structure at the atomic level (10^{-10}m range) [26]. The FEM solutions for the log SE with the Coulomb interaction are presented for the ground state and a number of excited states.

We also present variational results using linear combinations of (time-independent) Gaussons [27], that is, products of exponentials and Gaussians. (These should not be confused with the time-dependent Gaussons that are the free-particle solitonic solutions of the log SE.) Despite the simplicity of the basis, the energies and wave functions are remarkably close to the fully converged FEM solutions. Concluding remarks, commentary and discussion are presented at the end.

2. Theoretical model

The time-independent logarithmic Schrödinger equation with a Coulomb interaction can be expressed (in atomic units) as

$$\left[-\frac{1}{2}\nabla^2 - \frac{1}{r} - S\ln|\psi(S;\,\mathbf{x})| - \varepsilon(S)\right]\psi(S;\,\mathbf{x}) = 0, \tag{1}$$

where $\psi(S;\,\mathbf{x}) = \psi(S;\,r,\,\theta,\,\phi)$, S is a constant parameter, and $\varepsilon(S)$ is the total bound state energy. The system supports bound states only for $S \geqslant 0$. The log SE is not separable in the radial and θ coordinates. However, since $\ln|e^{im\phi}| = 0$, m remains a good quantum. We consider here the spherically symmetric case, where the wave function is independent of the angular coordinates, $\psi(S; r, \theta, \phi) = R(S; r)\, Y_0^0(\theta, \phi)$. The radial equation reduces to

$$\left[-\frac{1}{2}\frac{d^2}{dr^2} - \frac{1}{r}\frac{d}{dr} - \frac{1}{r} - S\ln|R_n| - E_n(S)\right]R_n(S;\,r) = 0\,, \tag{2}$$

where n is the principle quantum number and $E_n(S) = \varepsilon_n(S) - \frac{S}{2}\ln(4\pi)$. The Hamiltonian operator is nonlinear because it depends on the absolute value of the radial function, $|R_n(S;\,r)|$.

Note that the difference between E_n and ε_n is a direct consequence of the 3D nature of the problem. Experimentally, it is differences between energy states that are measured and for the same value of S, E_n and ε_n differ only by a constant (offset). This is true only for the special case when the wave function is independent of the angular coordinates. Moreover, if we make the rescaling $R(r) = \exp(-E_n/S)f(r)$, the energy $E_n(S)$ is eliminated [12, equation (18)] from (2)(although E_n appears in the normalization of $f(r)$). Hereafter, we refer to E_n as the energy, while the total bound state energy of the system is

$$\varepsilon_n(S) = E_n(S) + \tfrac{S}{2}\ln(4\pi). \tag{3}$$

The (non-degenerate) radial eigenfunctions of equation (2) are not orthogonal [11]. As shown in appendix A, they obey:

$$\langle R_n(S;\,r)|R_m(S;\,r)\rangle = S\frac{\langle R_n|\ln(|R_n|/|R_m|)|R_m\rangle}{(E_m - E_n)}, \tag{4}$$

where the integration is over the radial coordinate. The logarithmic interaction is pathologically non-linear: attractive for $|R_n| > 1$, repulsive for $0 \leqslant |R_n| < 1$, and singular at the nodes of the radial function.

2.1. Asymptotic behavior

For large r, equation (2) has the form:

$$\left[-\frac{1}{2}\frac{d^2}{dr^2} - \frac{1}{r}\frac{d}{dr} - S\ln|R_n| - E_n(S)\right]R_n(S;\, r) = 0. \tag{5}$$

Using the Maple computer algebra system [28], the leading asymptotic solution for equation (5) assuring square integrability for both the solution and its first derivative is given by:

$$R_n(S;\, r) \approx \exp\left(-\frac{S}{2}r^2 - CSr - \frac{SC^2}{2} - \frac{E_n}{S} + \frac{3}{2}\right), \tag{6}$$

where C is an arbitrary real constant. Note that $|R_n(S;\, r)| = R_n(S;\, r)$ for $0 < r < \infty$. Thus, asymptotically $R(r)$ has the general form:

$$R_n(S;\, r \to \infty) \to \exp\left(-\frac{S}{2}r^2 - b\, r\right), \tag{7}$$

where b may be a function of S. The functional form of equation (7) is that of a Gausson, i.e. the product of a Gaussian in r of the form $\exp\left(-\frac{S}{2}r^2\right)$ and what would seem like a Slater type function of the form $\exp(-br)$. Note, however, that since the Gaussian dominates the asymptotic behavior even for small S, the coefficient b need not be positive. Equation (7) expresses the asymptotic form of all the bound eigensolutions.

2.2. Ground state

Equation (2) is analytically solvable only for the ground state, where

$$E_1(S) = \frac{3}{2}S - \frac{1}{2} - S\ln(N_S), \tag{8}$$

$$R_1(S;\, r) = N_S \exp\left(-\frac{Sr^2}{2}\right)\exp(-r), \tag{9}$$

and the normalization factor is

$$N_S = \left[\frac{\sqrt{\pi}\,\exp\left(\frac{1}{S}\right)(2+S)\,\mathrm{erfc}\left(\frac{1}{\sqrt{S}}\right)}{4\,S^{5/2}} - \frac{1}{2S^2}\right]^{-1/2}, \tag{10}$$

where erfc is the complementary error function. Note that $R_1\,(S;r)$ of equation (9) is consistent with the asymptotic form of equation (7) for a single Gausson with $b = 1$. In the limit $S \to 0$, $E_1 = -1/2$, $N_S = 2$ and $R_1 = \exp\,(-r)$ which is indeed the ground state of the hydrogen atom. Using equation (8), and setting $\frac{dE_1(S)}{dS} = 0$, we find through symbolic manipulation with Maple that the ground state energy E_1 reaches a maximum when S is governed by:

$$\begin{aligned}
\mathrm{erfc}\,(1/\sqrt{S}) &= \frac{2\,S\,[W(k,\,-Y) + X] + S - 2}{\sqrt{S\pi}\,\exp(1/S)\,(S+2)\,W(k,\,-Y)},\\
X &= -\frac{1}{2}\,\frac{3S^2-4}{S(S+2)},\\
Y &= \frac{1}{2}\,\frac{\exp(-X)}{S(S+2)},
\end{aligned} \tag{11}$$

$W(k, x)$ is the Lambert W function [29–34] which satisfies $W\,(k,\,x)\exp(W\,(k,\,x)) = x$. The integer k refers to the particular branch. In this case, it is not the main branch at $k = 0$ but rather $k = -1$ for which $W(-1, x)$ is real valued on the interval $[-e^{-1},0]$. As predicted earlier [19, 22, 31], the Lambert W function does make its appearance in this body of work. Solving equation (11) leads to:

$$\begin{aligned}
S &= 0.640\,250059733\ldots\\
E_1^{\max} &= -0.302\,028005290\ldots
\end{aligned} \tag{12}$$

The relevance of this maximum (which also occurs for excited states) is not yet clear, since the bound state energy ε_n has no such feature. Nevertheless, it reflects a 'competition' between the Coulomb potential and the logarithmic term.

3. Computational aspects

3.1. FEM computational aspects

In order to gain insight into the analytical structure of the excited states, we solved equation (2) iteratively using the finite element approach. Details of the finite element method are given in [23–25], so we provide only a brief summary here.

In 1D finite element analysis, the continuum is truncated at $r_{\max}$, where the function and its derivative are required to vanish (we suppress the index n and the parameter S for clarity). The continuum $0 < r < r_{\max}$ is discretized into *nel* small regions called elements. In each element *iel*, the unknown radial wave function $R(r)$ is locally approximated by a sum of six 5th degree polynomials,

$$R^{iel}(r) = \sum_{j=1}^{6} c_j^{iel}\,\phi_j(x), \qquad -1 \leqslant x \leqslant 1. \tag{13}$$

The polynomials $\phi_j(x)$ have the property that the six unknown expansion coefficients c_j^{iel} are the value of $R(r)$ and dR/dr at the two endpoints and the midpoint of the *iel* element. Using equation (13) in equation (2) and projecting onto the basis functions, one obtains a 6×6 local matrix equation for each of the *nel* elements,

$$\sum_{i=1}^{6}\sum_{j=1}^{6} \langle \phi_i | \mathcal{H}^{iel} - E | \phi_j \rangle\, c_j^{iel} = 0. \tag{14}$$

With the exception of the logarithmic term, all of the integrals are simple polynomials and can be evaluated exactly. We used a 16-point Gauss quadrature to evaluate the logarithmic term. (We also carried out calculations at higher quadrature, to verify that the numerical integration was converged to the desired accuracy; see appendix B.) Imposing continuity of the wave function and its derivative across element boundaries (i.e., requiring that $c_5^{iel} = c_1^{iel+1}$, $c_6^{iel} = c_2^{iel+1}$) and enforcing the asymptotic boundary condition at $r_{\max}$ ($c_5^{nel} = c_6^{nel} = 0$) results in a generalized eigenvalue problem, where the two matrices are of order $4 \times nel$ with a bandwidth of 11. The resultant generalized eigenvalue problem was solved for the n^{th} eigenvalue only using a banded storage LAPACK routine DSBGVX. The solution yields the energy E_n and the expansion coefficients c_j^{iel} from which one can reconstruct a piecewise continuous function $R_n(S; r)$. For a given n, we find only the n^{th} eigenvalue and eigenfunction; the lower eigenvalues $l = 1, 2, \ldots, n-1$ are unphysical and correspond to the states which satisfy

$$\left[-\frac{1}{2}\frac{d^2}{dr^2} - \frac{1}{r}\frac{d}{dr} - \frac{1}{r} - S\ln|R_n| - E_l\right] R_l = 0. \tag{15}$$

Note that R_n appears in the log term, not R_l. These unphysical states obey the normal orthogonality condition since the effective potential is the same.

There are only two parameters in the finite element calculation; the value of $r_{\max}$ and the number of elements. This enables one to study convergence in a very systematic way. The FEM calculation is converged if increasing $r_{\max}$ (and keeping the element size the same) or increasing *nel* (and keeping $r_{\max}$ the same) does not change the value of the energy. The results of a typical convergence study are given in appendix B.

For the ground state calculation, the logarithmic term is ignored in the zeroth order iteration; that is, the equation is solved for the pure hydrogenic case. In the i^{th} iteration $i > 0$, the solution R_1^{i-1} is used in the logarithmic term. The energy is considered converged at the i^{th} iteration when $|E_1^{i+1} - E_1^i| < 10^{-13}$. The convergence table for $S = 1$ and $n = 1$ is shown in appendix B, table B1.

For the excited states, this simple iterative scheme is not sufficient due to the pathological nature of the logarithmic term at the nodes. A slight change in the position of the node moves the singularity. Although the convergence is initially monotonic, the energy begins to oscillate about the exact solution, and in some cases, the oscillations increase in amplitude. To correct this problem we use a weighted average of the last two iterations. For the zeroth iteration, the logarithmic term is ignored. For $0 < i \leqslant 10$, the solution R_n^{i-1} is used in the logarithmic term (as described above for the ground state). For $i > 10$, the weighted average $(I - i)\,R^{i-2}/I + i\,R^{i-1}/I$ is used in the logarithmic term. The value of I is increased until the convergence is monotonic. In general, the maximum number of iterations needed for convergence is roughly half the value of I. We emphasize that the value of I does not impact the final value for the energy, only the rate of convergence. For $n > 1$, the energy is considered converged at the i^{th} iteration when $|E_n^{i+1} - E_n^i| < 10^{-11}$. The convergence table for $S = 1$, $n = 3$ is shown in appendix B, table B2.

3.2. Variational principle

A preliminary analysis with Prony's method [35–37] suggests that the FEM solutions for $n = 2$ can be approximated as a sum of two Gaussons. For this analysis, we cast the Gausson sum into the form:

$$R_2(S;\, r) = N\, e^{-\frac{S}{2}r^2} e^{b_1 r}[1 + d_1 e^{b_2 r}], \tag{16}$$

where $N(S)$ is a normalization constant, $b_1\,(S)$ and $b_2\,(S)$ are free parameters, and $d_1\,(S)$ is uniquely determined by the nonorthogonality rule of equation (4). Although equation (16) is *not* the exact solution, it provides an excellent approximation to the FEM wave function over the full range $0 < r < \infty$. We further note that an error in the wave function of order δ gives rise to an error in the energy of the same order δ. This is in contrast to the linear Hamiltonian case, where the error in the energy is δ^2. We note that the proof for the linear operator relies on the orthogonality of the wave function, which does not hold in this case.

In calculating the expectation value of the Hamiltonian $\langle R_2|\mathcal{H}|R_2\rangle$, all of the integrals can be evaluated exactly with the exception of the logarithmic term, which leads to integrals of the form

$$\int_0^\infty r^k e^{-Sr^2+B\,r}\, \ln|1 + d_1 e^{b_2 r}|\, dr, \tag{17}$$

where k is a positive integer and B is some combination of b_1 and b_2. For the $n = 2$ excited state, d_1 is negative and thus the integral in (17) is a Cauchy principal value. The nonorthogonality condition between the $n = 2$ state and the ground state also leads to such integrals. The class of integrals of (17) have no known analytical solutions and the derivatives with respect to the free parameters are even more unwieldy.

As an alternative, we use the hybrid symbolic-methods [38–40], in particular the generation of optimized MATLAB code [41] to apply the variational principle. We used MATLAB functions to numerically solve all the integrals of the class in (17) but *all* other integrals are solved analytically using Maple. Since derivatives of the integrals in (17) with respect to the parameters b_2 and d_1 are problematic, to find the minimum energy, we compute the expectation values for the energy $\langle R_2|\mathcal{H}|R_2\rangle$ over a fine grid of values b_1 and b_2 with d_1 being determined from the nonorthogonality condition of (4). We then select the minimum, subject to the constraint that N ensures that R_2 is normalized to unity.

The nested loops over the parameters b_1 and b_2 are computationally expensive. However, the double loop over grid values of b_1 and b_2 can be reduced to a *single* loop over b_1, by using the value of the $n = 2$ node obtained from the FEM results. Requiring $R_2\,(S, x) = 0$, implies $d_1 = -e^{-b_2 x}$, where x is the value of the node; b_2 is no longer a free parameter. The parameters d_1 and b_2 can now be found simultaneously with the nonorthogonality condition using MATLAB's `fzero` root solver function.

This approach can be extended to excited states using the sum of Gaussons:

$$R_n(S;\, r) \;=\; N e^{-\frac{S}{2}r^2} e^{b_1 r}\left[1 + \sum_{i=1}^{n-1} d_i e^{b_{i+1} r}\right] \tag{18}$$

Of the $2n$ S-dependent parameters, N is fixed by normalization, and the $(n - 1)$ values of d_i are constrained by the nonorthogonality condition of equation (4). This leaves only n free parameters, b_i, $i = 1, 2, \ldots, n$; however, the nested loops over the parameters b_i become computationally prohibitive for $n > 2$. We therefore employ the method described above for $n = 2$, and use the known value of the $(n - 1)$ nodes to collapse the problem to a single loop over b_1. For example, for the state $n = 3$,

$$\begin{aligned} d_1 &= \frac{e^{b_3 x_1} - e^{b_3 x_2}}{e^{b_2 x_1 + b_3 x_2} - e^{b_2 x_2 + b_3 x_1}}, \\ d_2 &= \frac{e^{b_2 x_2} - e^{b_2 x_1}}{e^{b_2 x_1 + b_3 x_2} - e^{b_2 x_2 + b_3 x_1}}, \end{aligned} \tag{19}$$

where x_1 and x_2 are the two radial nodes for the $n = 3$ wave function (see table 3).

4. Numerical results

4.1. Finite element results

Our goal is to obtain energy levels that are accurate to better than one part in 10^{10} for $n = 1$, and better than one part in 10^8 for $n > 1$. All calculations were carried out in double precision. In table 1, we compare the FEM results with the exact energy $E_1\,(S)$ given in equation (8). FEM results for $n = 2, 3$ and 4 are given in tables 2–4, respectively; we include both the energies $E_n\,(S)$ and the position of the nodes. There is a well-defined maximum in $E_n\,(S)$, (but not in $\varepsilon_n\,(S)$). The energies for $n = 1, 2, 3$, and 4 are plotted as a function of S in figure 1. One important check on the accuracy of the FEM wave functions was the nonorthogonality condition. We stress that we did not enforce equation (4) a prior, but found each state in a separate calculation. In table 5, we compare the value of $\langle R_n(r)|R_m(r)\rangle$ with equation (4). It is an important feature of this approach that the FEM wave functions automatically satisfy the nonorthogonality condition.

In figure 2, we show the radial function for $n = 4$ for $S = 0, 0.5, 1, 2$ and 5. The logarithmic term is responsible for a dramatic compression of the wave function towards the origin.

Table 1. Comparison of the exact energies $E_1(S)$ and FEM results (in atomic units). The energy maximum is $E_1(0.640\ 25) = -0.302\ 0\ 28005$.

S	$E_1(S)$ [Exact]	$E_1(S)$ [FEM]
0.00	−0.500 0 0000 00	−0.500 0 0000 00
0.25	−0.363 6 6012 08	−0.363 6 6012 08
0.50	−0.309 0 9134 08	−0.309 0 9134 08
0.75	−0.305 9 6626 39	−0.305 9 6626 39
1.00	−0.341 1 6113 23	−0.341 1 6113 23
1.50	−0.498 8 1741 44	−0.498 8 1741 44
2.00	−0.746 2 4996 09	−0.746 2 4996 09
3.00	−1.439 8 7398 83	−1.439 8 7398 83
4.00	−2.333 6 8142 68	−2.333 6 8142 68
5.00	−3.381 7 9756 31	−3.381 7 9756 31
6.00	−4.555 8 2070 96	−4.555 8 2070 96
7.00	−5.836 3 4743 50	−5.836 3 4743 50
8.00	−7.209 2 4633 98	−7.209 2 4633 98
9.00	−8.663 7 5018 21	−8.663 7 5018 21
10.00	−10.191 3 7383 44	−10.191 3 7383 44

Table 2. FEM results for $E_2(S)$ (in atomic units). x is the location of the node. The energy maximum is $E_2(5.669\ 1) = 3.455\ 8\ 4120$.

S	$E_2(S)$	x
0.0	−0.125 0 0000	2.000 0
0.5	0.846 3 6276	1.411 5
1.0	1.498 2 7745	1.171 9
2.0	2.385 9 4477	0.932 9
3.0	2.939 6 2535	0.803 4
4.0	3.268 7 2719	0.718 3
5.0	3.427 6 6806	0.656 6
6.0	3.449 3 3063	0.609 1
7.0	3.355 8 1688	0.571 0
8.0	3.163 0 3283	0.539 5
9.0	2.882 9 8677	0.512 9
10.0	2.525 0 7200	0.490 0

Table 3. FEM results for $E_3(S)$ (in atomic units). x_1 and x_2 are the location of the nodes. The energy maximum is $E_3(14.196) = 9.813\ 6\ 5841$.

S	$E_3(S)$	x_1	x_2
0.0	−0.055 5 5556	1.901 9	7.098 1
0.5	1.325 8 0070	1.281 8	3.819 3
1.0	2.339 0 0895	1.053 7	3.001 8
2.0	3.919 0 3634	0.832 6	2.289 6
3.0	5.147 8 0196	0.714 6	1.933 4
4.0	6.142 9 8838	0.637 7	1.708 3
5.0	6.962 2 4752	0.582 2	1.549 0
6.0	7.640 1 2679	0.539 6	1.428 3
7.0	8.199 7 1910	0.505 5	1.332 8
8.0	8.657 5 7696	0.477 5	1.254 6
9.0	9.026 1 5804	0.453 6	1.189 0
10.0	9.315 1 8316	0.433 2	1.133 0

4.2. Variational principle

The results of the variational calculation, i.e. the parameters for the ansatz of (16), for the $n = 2$ state are tabulated in table 6 as a function of S; the values are rounded to 6 digits. These were obtained according to the method in subsection 3.2 using the nodes from the FEM results as tabulated in table 2. Note that these results

Table 4. FEM results for $E_4(S)$ (in atomic units). x_i, $i = 1, 2, 3$ are the location of the nodes.

S	$E_4(S)$	x_1	x_2	x_3
0.0	−0.031 2 5000	1.871 6	6.610 8	15.517 5
0.5	1.624 4 4651	1.220 5	3.420 0	6.648 8
1.0	2.882 6 6851	0.996 7	2.679 1	5.081 6
2.0	4.936 5 1846	0.783 5	2.039 3	3.798 1
3.0	6.629 9 3004	0.671 1	1.720 7	3.178 2
4.0	8.085 0 2230	0.598 0	1.519 6	2.793 0
5.0	9.361 1 5941	0.545 5	1.377 6	2.523 3

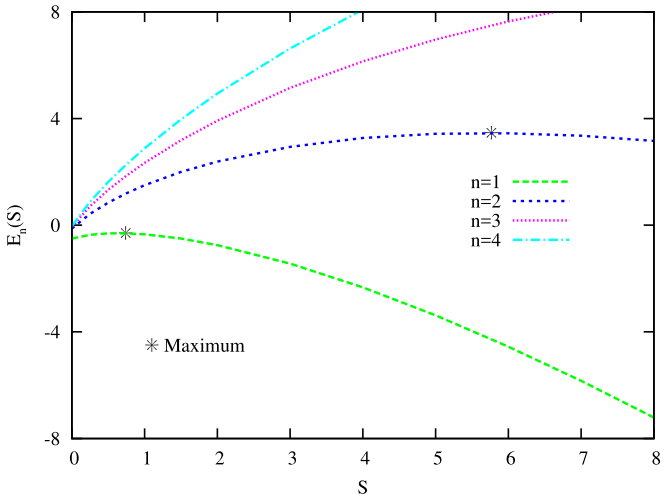

Figure 1. The values of $E_n(S)$ (in atomic units) are shown as a function for S for $n = 1$,2,3 and 4.

Table 5. Verification of the nonorthogonality condition for $R_n(S = 1; r)$ for $n = 1, 2, 3, 4$. These results were obtained using the same FEM grid, to facilitate the evaluation of integrals between different states could be carried out easily.

n	m	$\langle R_n(r) \vert R_m(r)\rangle$	$\frac{\langle R_n \vert \ln(\vert R_n \vert / \vert R_m \vert) \vert R_m\rangle}{(E_m - E_n)}$
1	2	0.217 43	0.217 44
1	3	0.104 74	0.104 75
1	4	0.064 45	0.064 46
2	3	0.379 82	0.379 83
2	4	0.161 36	0.161 36
3	4	0.457 29	0.457 29

were confirmed without using the nodes by a more laborious calculation over grids for both the b_1 and b_2 parameters essentially confirming the same outcome.

As S gets larger in magnitude, absolute discrepancies between the FEM and variational results increase, although the relative error decreases: for $S = 5$, $\Delta E = 0.02$ (0.6 %) and for $S = 0.05$, $\Delta E = 10^{-4}$ (2 %). As we can see from table 6, the b_1 coefficient becomes negative at around $S \approx 0.05$ and d_1 becomes smaller in magnitude as S approaches zero, thus ensuring the correct $S \to 0$ limit. Figure 3 shows how well the variational function fits the FEM wave function to within plotting accuracy for three different values of S, i.e. $S = 1, 2$ and 5. In figure 4, we plot the parameters as function of S. The magnitude of b_1 and b_2 appear to grow almost logarithmically with S

In figures 5 and 6, we compare the variational wavefunction obtained from the ansatz equation (18) with the FEM wave function for the states $n = 3$ and $n = 4$. We used the nodes given in tables 3 and 4 to reduce the number of free parameters to one. It is clear that the variational wave function is within plotting accuracy of the accurate FEM result. As expected, the variational energies lies slightly above the FEM energies.

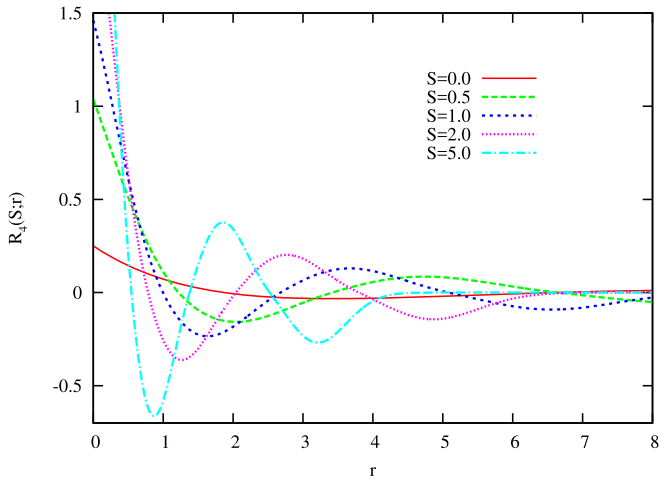

Figure 2. $R_4(S;r)$ versus the radius r for $S = 0, 0.5, 1, 2$ and 5.

Table 6. Variational parameters of equation (18) for the $n = 2$ state.

S	$E_2(S)$ [FEM]	$E_2(S)$ [var]	N	b_1	b_2	d_1
0.05	0.004 7 4275	0.004 8 4810	−0.501 326	−0.159	−0.528 847	−2.731 690
0.1	0.121 4 2956	0.121 7 0859	−0.311 946	0.036	−0.787 606	−4.176 502
0.6	0.993 3 1446	0.995 5 8511	−0.100 137	1.185 6	−2.182 742	−19.050 690
1.0	1.498 2 7745	1.502 1 6393	−0.080 718	1.791 6	−2.884 749	−29.397 966
2.0	2.385 9 4477	2.393 9 4357	−0.068 202	2.923 2	−4.175 252	−49.181 138
3.0	2.939 6 2535	2.951 8 0206	−0.066 435	3.795 2	−5.165 432	−63.297 230
4.0	3.268 7 2719	3.285 1 3128	−0.066 918	4.534 5	−5.998 009	−74.185 621
5.0	3.427 6 6806	3.448 3 3018	−0.067 796	5.193 5	−6.731 189	−83.295 213

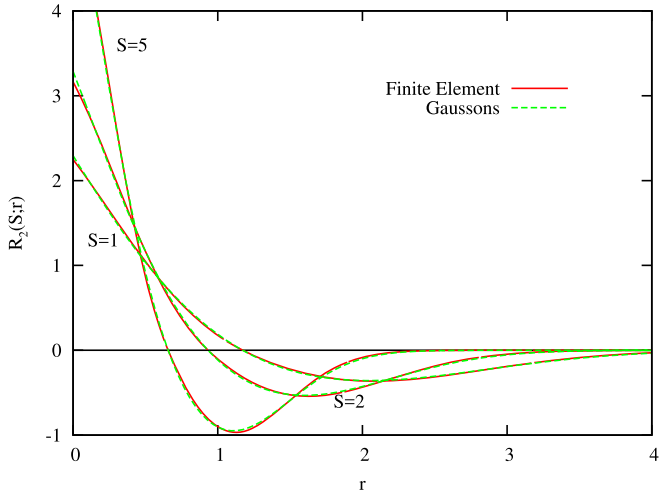

Figure 3. $R_2(S, r)$ fitted to the sum of two Gaussons for $S = 1, 2$ and 5 using the parameters of table 6.

5. Discussion

In summary, we have obtained an analytical solution to the ground state for the log SE with a Coulomb interaction. For the spherically symmetric case, the FEM method yields extremely accurate solutions for the low-lying bound states. A simple variational wave function consisting of a sum of n Gaussons is shown to provide an excellent approximation for the excited states. This is particularly important because the most developed industry for quantum chemistry calculations employs Gaussians and Slater type functions (see [38–40] and

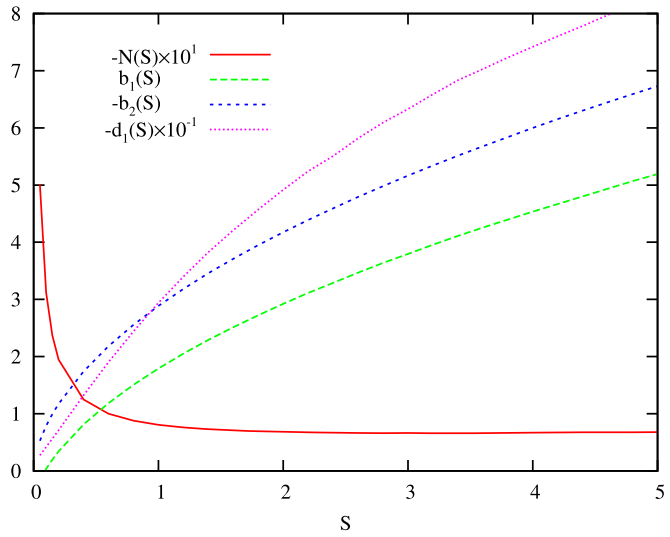

Figure 4. Variational parameters for $n = 2$ as a function of S.

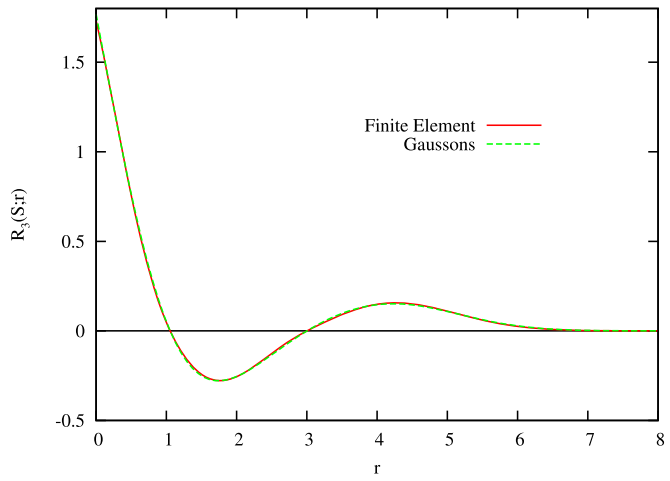

Figure 5. $R_3(S, r)$ fitted to the sum of three Gaussons using equation (18) with $b_1 = 4.150\ 5, b_2 = -5.047\ 6, b_3 = -2.992\ 3$, $d_1 = 7.048\ 9 \times 10^4, d_2 = -8.106\ 9 \times 10^3$ and $N_3 = 2.834\ 0 \times 10^{-5}, E_3 = 2.343\ 6$ for $S = 1$.

references therein). This suggests that many of the computational tools developed in quantum chemistry may be relevant even in the presence of the highly non-linear logarithmic term.

We have considered the spherically symmetric case with a Coulomb potential. From here, a number of investigations with our numerical methods can be contemplated. First, the central potential used in the FEM calculation can easily be modified; for example, one could consider potentials that arise in quantum gravity or the Higgs potential, as discussed in the Introduction. Since the asymptotic behavior is dominated by the logarithmic term, it is expected that the Gaussons will continue to serve as an excellent variational basis. An equally challenging problem is to consider the 1D continuum states of the log SE with a Coulomb interaction (or other central potential).

In order to go beyond the spherically symmetric case, 2D FEM can be used to solve the log SE in the variables r and θ for fixed m, which remains a good quantum number for a central potential. In the 2D case, the logarithmic term diverges along the nodal lines. The number of nodal lines will increase with increasing energy. In the limit $S \rightarrow 0$, the nodal lines must approach the correct hydrogenic limit, and the two new quantum numbers must collapse into n and ℓ.

Finally, the iterative approach developed here, which ensures monotonic convergence, could potentially be applied to the Gross-Pitaevski equation or to other nonlinear differential eigenvalue equations in field theory.

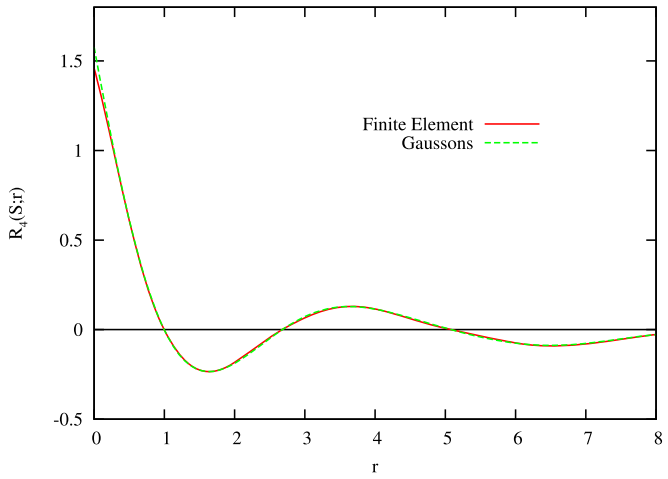

Figure 6. $R_4(S, r)$ wave function fitted to the sum of four Gaussons using ansatz of (18) with $b_1 = 3.350\,0$, $b_2 = -2.170\,2$, $b_3 = 3.108\,6$, $b_4 = -4.409\,4$, $d_1 = -3.425\,2 \times 10^2$, $d_2 = -1.371\,6 \times 10^{-7}$, $d_3 = 3.110\,0 \times 10^3$, $N_4 = 5.698\,1 \times 10^{-4}$, $E_4 = 2.888\,2$ for $S = 1$.

Acknowledgments

T C Scott would like to thank Greg Fee of the Centre for Experimental and Constructive Mathematics (CECM), Simon Fraser University, Burnaby, British Columbia, Canada for suggesting the Prony method. T C Scott would like to thank Konstantin G. Zloshchastiev of the University of KwaZulu-Natal in Pietermaritzburg, South Africa, Weizhu Bao of the National University of Singapore, Professor B. Ananthanarayan of the Centre for High Energy Physics, Indian Institute of Science (IISC) in Bangalore, India, and Yehuda Band of the Ben-Gurion University in the Negev, Israel and NYU Shanghai, China for their invaluable discussions and insight. T C Scott would also like to thank Madhusudan Therani, Principal of EngKraft LLC and Arne Lüchow of the Institut für Physikalische Chemie at RWTH-Aachen University for their support. J Shertzer gratefully acknowledges the technical assistance provided by Richard Nickle, Senior Technical Services Engineer, Information Technology Services, College of the Holy Cross.

Appendix A. Derivation of the nonorthogonality condition

Consider two normalized solutions to equation (2), with $m > n$:

$$\left[-\frac{1}{2}\frac{d}{dr^2} - \frac{1}{r}\frac{d}{dr} + V(r) - S\ln|R_n| - E_n\right]R_n = 0 \tag{A.1}$$

$$\left[-\frac{1}{2}\frac{d}{dr^2} - \frac{1}{r}\frac{d}{dr} + V(r) - S\ln|R_m| - E_m\right]R_m = 0. \tag{A.2}$$

Taking the inner product of (A.1) with R_m and (A.2) with R_n, one obtains

$$\langle R_m|\left[-\frac{1}{2}\frac{d}{dr^2} - \frac{1}{r}\frac{d}{dr} + V(r) - S\ln|R_n| - E_n\right]|R_n\rangle = 0 \tag{A.3}$$

$$\langle R_n|\left[-\frac{1}{2}\frac{d}{dr^2} - \frac{1}{r}\frac{d}{dr} + V(r) - S\ln|R_m| - E_m\right]|R_m\rangle = 0. \tag{A.4}$$

Subtracting (A.4) from (A.3), and exploiting the Hermiticity of the kinetic and potential energy operators, only two terms remain:

$$(E_m - E_n)\langle R_n|R_m\rangle - S\langle R_n|\ln(|R_n|/|R_m|)|R_m\rangle = 0.$$

Since $E_m > E_n$, the nonorthogonality condition is given by

$$\langle R_n|R_m\rangle = S\frac{\langle R_n|\ln(|R_n|/|R_m|)|R_m\rangle}{(E_m - E_n)}. \tag{A.5}$$

Table B1. Convergence study for the ground state $n = 1, S = 1$. r_{max} is the radial cutoff (in atomic units). *nel* is the total number of elements and $\Delta r = r_{max}/nel$ is the size of the element. N is the order of the Gauss quadrature. i is the iteration number. The results are considered converged when $|E_1^{i+1} - E_1^i| < 10^{-13}$; the value of i (at convergence) is recorded in the table. For $n = 1$, the radial function from the previous iteration $R^{i-1}(r)$ was used in the logarithmic term.

r_{max} (a.u.)	*nel*	Δr (a.u.)	N	i	CPU (sec)	E_1 (a.u.)
4.0	4	1.0	16	16	0.01	−0.341 1 6101 1938
5.0	5	1.0	16	16	0.01	−0.341 1 6107 3036
6.0	6	1.0	16	16	0.01	−0.341 1 6107 3045
7.0	7	1.0	16	16	0.01	−0.341 1 6107 3045
6.0	6	**1.0**	16	16	0.01	−0.341 1 6107 3045
6.0	12	**0.5**	16	16	0.01	−0.341 1 6113 2216
6.0	30	**0.2**	16	18	0.07	−0.341 1 6113 2279
6.0	60	**0.1**	16	15	0.30	−0.341 1 6113 2278
6.0	60	0.1	**8**	19	0.30	−0.341 1 6113 2278
6.0	60	0.1	**16**	15	0.37	−0.341 1 6113 2278
6.0	60	0.1	**24**	39	0.80	−0.341 1 6113 2279
6.0	60	0.1	**32**	15	0.32	−0.341 1 6113 2278
6.0	60	0.1	**40**	21	0.46	−0.341 1 6113 2278
					FEM	−0.341 1 6113 23
					Exact	−0.341 1 6113 2278

Table B2. Convergence study for the ground state $n = 3, S = 1$. r_{max} is the radial cutoff (in atomic units). *nel* is the total number of elements and $\Delta r = r_{max}/nel$ is the size of the element. N is the order of the Gauss quadrature. i is the iteration number; the results are considered converged when $|E_1^{i+1} - E_1^i| < 10^{-13}$, and the value of i (at convergence) is recorded in the table. For $n > 1$, the radial function from the previous iteration $R^{i-1}(r)$ was used in the logarithmic term for the first 10 iterations. Thereafter, we used a weighted average of the last two iterations to ensure monotonic convergence: $(I - i)R^{i-2}/I + iR^{i-1}/I$. It was necessary to increase I with increasing n and S; the value of I does not change the result, only the convergence rate.

r_{max} (a.u.)	*nel*	Δr (a.u.)	N	I	i	CPU (min:sec)	E_1 (a.u.)	Node 1	Node 2
8.0	40	0.2	16	600	286	00:02	2.339 0 0947 2988	1.503 6 98	3.001 7 45
9.0	45	0.2	16	600	275	00:02	2.339 0 0873 6601	1.503 6 99	3.001 7 52
10.0	50	0.2	16	600	291	00:03	2.339 0 0873 6474	1.503 6 99	3.001 7 56
11.0	55	0.2	16	600	279	00:04	2.339 0 0873 6474	1.503 6 99	3.001 7 56
12.0	60	0.2	16	600	288	00:06	2.339 0 0873 6473	1.503 6 99	3.001 7 55
11	55	**0.2**	16	600	279	00:04	2.339 0 0873 6476	1.503 6 99	3.001 7 55
11	110	**0.1**	16	600	282	00:34	2.339 0 0892 6462	1.503 6 95	3.001 7 57
11	220	**0.05**	16	600	260	04:23	2.339 0 0895 0956	1.503 6 91	3.001 7 54
11	440	**0.025**	16	600	269	49:37	2.339 0 0895 1234	1.503 6 91	3.001 7 52
11	220	0.05	**16**	600	260	04:23	2.339 0 0895 0956	1.503 6 91	3.001 7 54
11	220	0.05	**24**	600	265	04:40	2.399 0 0895 1257	1.503 6 91	3.001 7 53
11	220	0.05	**32**	600	284	04:49	2.399 0 0895 1006	1.503 6 91	3.001 7 50
11	220	0.05	**40**	600	256	04:21	2.399 0 0895 1154	1.503 6 92	3.001 7 50
11	220	0.05	**48**	600	262	04:26	2.399 0 0895 1109	1.503 6 92	3.001 7 54
11	220	0.05	**60**	600	275	04:44	2.399 0 0895 1096	1.503 6 91	3.001 7 51
						FEM	2.399 0 0895	1.503 7	3.001 7 5

Appendix B. Convergence Study

The only parameters in the FEM calculation are the value of the cutoff radius r_{max} and the size of the elements. The convergence study for the ground state at $S = 1$ is shown in table B1. We also verify the accuracy of the Gauss quadrature. With only four elements, the energy is accurate to one part in 10^6.

For the excited states, it is necessary to introduce a weighted average of the last two iterations in order to obtain monotonic convergence. The weighting parameter does not affect the final value of the energy, only the rate of convergence. Results for the state $n = 3$ and $S = 1$ are shown in table B2. The convergence with respect to the Gauss quadrature is not strictly monotonic because the accuracy is slightly dependent on location of the sampling points relative to the nodes.

ORCID iDs

T C Scott https://orcid.org/0000-0002-0228-1673

References

[1] Buljan H, Šiber A, Soljačić M, Schwartz T, Segev M and Christodoulides D N 2003 *Phys. Rev.* E **68** 036607
[2] Znojil M, Ružička F and Zloshchastiev K G 2017 *Symmetry* **9**
[3] Hefter E F 1985 *Phys. Rev.* A **32** 1201–4
[4] Kartavenko V G, Gridnev K A and Greiner W 1998 *Int. J. Mod. Phys.* E **07** 287–99
[5] Hansson T, Anderson D and Lisak M 2009 *Phys. Rev.* A **80** 033819
[6] Lemos N A 1980 *Phys. Lett.* A **78** 239–41
[7] Zloshchastiev K G 2010 *(G & C) Gravitation and Cosmology* **16** 288–97
[8] Bao W 2011 *The Nonlinear Schrödinger Equation and Applications in Bose–Einstein Condensation and Plasma Physics* (Singapore: World Scientific) pp 141–239
[9] Zloshchastiev K G 2011 *Acta Phys. Polon.* B **42** 261–92
[10] Rosen G 1969 *Phys. Rev.* **183** 1186–8
[11] Bialynicki-Birula I and Mycielski J 1976 *Ann. Phys.* **100** 62–93
[12] Bialynicki-Birula I and Mycielski J 1979 *Phys. Scr.* **20** 539
[13] Bialynicki-Birula I and Sowiński T 2005 *Solutions of the Logarithmic Schrödinger Equation in a Rotating Harmonic Trap* (Dordrecht: Springer Netherlands) pp 99–106
[14] Volovik G E 2005 *JETP* **82** 319–24
[15] Zloshchastiev K G 2012 *Eur. Phys. J.* B **85** 273
[16] Dzhunushaliev V and Zloshchastiev K G 2013 *Open Phys.* **11** 325–35
[17] Dzhunushaliev V, Makhmudov A and Zloshchastiev K G 2016 *Phys. Rev.* D **94** 096012
[18] Bellazzini B, Csaki C, Hubisz J, Serra J and Terning J 2013 *Eur. Phys. J.* C **73** 2333
[19] Scott T C, Zhang X, Mann R B and Fee G J 2016 *Phys. Rev.* D **93** 084017
[20] Kimura T 1961 *Prog. Theor. Phys.* **26** 157
[21] Ohta T, Okamura H, Kimura T and Hiida K 1974 *Prog. Theor. Phys.* **51** 1598–612
[22] Farrugia P S, Mann R B and Scott T C 2007 *Class. Quantum Grav.* **24** 4647
[23] Bathe K J and Wilson E L 1976 *Numerical Methods in Finite Element Analysis* (Englewood Cliffs, NJ: Prentice-Hall)
[24] Ram-Mohan L R 2002 *Finite Element and Boundary Element Applications in Quantum Mechanics (Oxford Texts in Applied and Engineering Mathematics)* (Oxford: Oxford University Press)
[25] Ram-Mohan L R, Saigal S, Dossa D and Shertzer J 1989 *Comput. Phys.* **4** 50–9
[26] Scott T C, Shertzer J and Moore R A 1992 *Phys. Rev.* A **45** 4393–8
[27] Goldin G A and Svetlichny G 1994 *Nonlinear Quantum Mechanics, the Separation Property, and a Stochastic Alternative to Certain Nonlinear Schrödinger Equations* (Boston, MA: Springer US) pp 245–55
[28] Bernardin L *et al* 2012 *Maple Programming Guide* (Toronto: Maplesoft, a division of Waterloo Maple, Inc.)
[29] Corless R M, Gonnet G H, Hare D E G and Jeffrey D J 1993 *MapleTech* **9** 12–22
[30] Corless R M, Gonnet G H, Hare D E G, Jeffrey D J and Knuth D E 1996 *Adv. Comput. Math.* **5** 329–59
[31] Scott T C, Mann R and Martinez R E II 2006 *AAECC (Applicable Algebra in Engineering, Communication and Computing)* **17** 41–7
[32] Scott T C, Fee G and Grotendorst J 2014 *ACM Commun. Comput. Algebra* **47** 75–83
[33] Scott T C, Fee G, Grotendorst J and Zhang W Z 2014 *ACM Commun. Comput. Algebra* **48** 42–56
[34] Maignan A and Scott T C 2016 *ACM Commun. Comput. Algebra* **50** 45–60
[35] Carriere R and Moses R L 1992 *IEEE Trans. Antennas Propag.* **40** 13–8
[36] Hauer J F, Demeure C J and Scharf L L 1990 *IEEE Trans. Power Syst.* **5** 80–9
[37] Marple S L 1987 *Digital Spectral Analysis With Applications* (Australia, Sydney: Prentice Hall)
[38] Scott T C, Grant I P, Monagan M B and Saunders V R 1997 *MapleTech* **4** 15–24
[39] Scott T, Monagan M, Grant I and Saunders V 1997 *Nucl. Instrum. Methods Phys. Res. A* **389** 117–20
[40] Gomez C and Scott T 1998 *Comput. Phys. Commun.* **115** 548–62
[41] Scott T and Zhang W 2015 *Comput. Phys. Commun.* **191** 221–34